J2.8

CHARACTERISTICS OF WATER CLOUD OPTICAL PROPERTY AS SIMULATED BY A NON-HYDROSTATIC SPECTRAL MICROPHYSICS CLOUD MODEL

*Kentaroh Suzuki and Teruyuki Nakajima
Center for Climate System Research, University of Tokyo, Chiba, Japan

Takashi Y. Nakajima
Tokai University, Tokyo, Japan

Hirohiko Masunaga and Toshihisa Matsui
Colorado State University, Fort Collins, Colorado

Alexander P. Khain
Hebrew University of Jerusalem, Jerusalem, Israel

1. Introduction

Clouds are recognized as a major source of uncertainty in the assessment of climate change. The radiative effect of clouds plays a fundamental role in the climate system, and thus the cloud optical property is a key factor for determining the cloud radiative effect on climate. In this regard there have been many previous remote sensing studies of the cloud optical thickness and effective particle radius, which are main parameters to determine the cloud property, from aircraft measurement (Nakajima and King, 1990; Nakajima et al., 1991; Asano et al., 1995; Brenguier et al., 2000) and satellite image analysis (Han et al., 1994; Nakajima and Nakajima, 1995; Kawamoto et al., 2001). These two parameters, by their definitions, are determined by the size distribution function of cloud particles and thus strongly depend on the cloud microphysical structure, which is recognized to depend on both aerosol amount and dynamical condition (Matsui et al., 2004). The combination of optical thickness and effective radius, therefore, contains useful information of the cloud particle growth process and provides a key link between cloud radiative property and microphysical characteristics of the cloud system.

The correlation pattern between cloud optical thickness and effective radius of low-level clouds has been investigated by past several studies based on remote sensing results (Han et al., 1994, 1998; Asano et al., 1995; Boers and Rotstayn, 2001; Nakajima and Nakajima, 1995; Kawamoto et al., 2001; Szczodrak et al., 2001; Peng et al., 2002), since Nakajima et al. (1991) discovered that these optical parameters are positively correlated when the cloud is not drizzling and negatively correlated when the cloud includes a significant concentration of drizzle droplets.

Corresponding author address: Dr. Kentaroh Suzuki, Center for Climate System Research, University of Tokyo, 5-1-5 Kashiwanoha, Kashiwa, Chiba 277-8568, JAPAN; e-mail: kenta@ccsr.u-tokyo.ac.jp

The positive correlation for non-drizzling cloud means that the cloud becomes optically thicker with particle growth possible due to loss of the cloud water by conversion to drizzle or rain water. Nakajima and Nakajima (1995) investigated the correlation patterns over the FIRE (First ISCCP Regional Experiment) and ASTEX (Atlantic Stratocumulus Transition Experiment) region, and found that the correlation pattern seems to be different between over these two regions. The FIRE region has more negative correlation than the ASTEX region, implying that drizzle-rich clouds are dominant over the FIRE region.

The recent remote sensing study with combined use of visible-infrared scanner (VIRS) and microwave imager (TMI) aboard the TRMM satellite retrieved two kinds of effective radius of water cloud (Masunaga et al., 2002a,b; Matsui et al. 2004). One is an effective radius near the cloud top r_e(top) derived from the analysis of VIRS data based on the traditional algorithm of Nakajima and King (1990). Another is a column-averaged effective radius r_e(column), which is determined from the microwave-retrieved liquid water path and the visible-derived optical thickness. The value of r_e(column) thus determined contains the signal of drizzle particles because the mass of drizzle particles significantly contributes to the microwave-derived liquid water path. The combination of r_e(top) and r_e(column) enables us to get information of vertical stratification of cloud particles. It is expected that the value of r_e(column) is smaller than that of r_e(top) for non-drizzling clouds because the cloud particle tends to grow with height in such clouds. For drizzling clouds, on the contrary, the value of r_e(column) is greater than that of r_e(top) because there tends to exist the significant concentration of drizzle particles in lower layer of those clouds. In fact the global distributions of r_e(column) and r_e(top) retrieved from the TRMM analysis revealed the climatology of warm clouds, which corresponds to the climatology of rainfall (Masunaga et al., 2002b; Matsui et al., 2004). Matsui et al. (2004) investigated the scatter plot of r_e(top) and r_e(colulmn) obtained

from the global analysis, and showed that these two parameters are differently correlated for small and large values of r_e(top). The value of r_e(column) slowly increases with r_e(top) over the size range of r_e(top) smaller than 15um, corresponding to non-drizzling clouds, whereas the r_e(column) rapidly increases with r_e(top) over the size range of r_e(top) larger than 15μm, corresponding to drizzling clouds. The transition of correlation curve of r_e(column) and r_e(top) can be attributed to the difference in dominant process responsible for particle growth between non-drizzling and drizzling clouds.

Modeling study will be useful for investigating the formation mechanisms of these correlation patterns between effective radius and optical thickness and also between r_e(top) and r_e(column). In this study we performed numerical experiments with a non-hydrostatic spectral microphysics cloud model to simulate the correlation patterns. Because the spectral microphysics cloud model explicitly predicts the size distribution function of cloud particles, the simulated results provides us with detailed insight into the mechanisms underlying the correlation patterns.

2. Model simulation

In order to investigate the cloud microphysical processes in detail we adopted the non-hydrostatic spectral bin cloud microphysics model, which has been reconstructed from the original model of Khain and Sednev (1996) and Khain et al. (2004). In this model the size distribution function of liquid cloud particles $f(m,t)$ is explicitly predicted taking into account the various microphysical processes, i.e. nucleation from aerosol, condensational growth and collision-coagulation process.

The nucleation process is calculated from the size distribution function of hygroscopic aerosols, which is also predicted in the model. We prepared 20 bins ranging from 0.01μm to 1μm for aerosol size spectra and 60 bins from 3μm to 3000μm for cloud particle size spectra. The part of aerosol population greater than the critical size is activated to grow into cloud particles. This critical radius of aerosol is calculated from the supersaturation according to the Kohler theory. The sulfate aerosol (ammonium sulfate) was assumed for chemical species in the simulation. The number concentration of aerosols beyond the critical size is added to the minimum size bin of cloud particle (3μm). The number of aerosols belonging to size bins greater than the critical size becomes zero after the nucleation.

The nucleated cloud particle grows by condensation and collision-coagulation processes in the model. The prognostic equation for cloud size spectra by these processes is given as (e.g. Rogers and Yau, 1989)

$$\frac{\partial}{\partial t} f(m,t) = -\frac{\partial}{\partial m}\left(f(m,t)\frac{dm}{dt} \right) + \frac{1}{2}\int_0^m f(m',t) f(m-m',t) K(m',m-m') dm' - f(m,t)\int_0^{+\infty} f(m',t) K(m,m') dm' ,$$

where m denotes the mass of a cloud particle and t denotes the time. The first term on the right hand side represents the condensation process, and the second and third terms represent the collision-coagulation process. The growth speed of condensation is determined by supersaturation S as

$$\frac{dm}{dt} = rG(p,T)S , \qquad (1)$$

where r denotes the particle radius and $G(p,T)$ is a function of pressure p and temperature T given as

$$G(p,T) = \frac{4\pi}{\left[\left(\frac{L}{R_v T} - 1 \right) \frac{L}{KT} + \frac{R_v T}{De^*(T)} \right]} ,$$

where L, R_v, K, D and $e^*(T)$ are the latent heat, gas constant for water vapor, thermal conductivity, diffusion coefficient for water vapor and saturation vapor pressure at temperature T, respectively. The growth speed is positive (condensation) when the supersaturation S is positive and negative (evaporation) when the supersaturation S is negative. The supersaturation S is determined from the balance between condensation or evaporation and cooling of air by upward motion. The collection kernel function $K(m_1,m_2)$ for the collision-coagulation process is assumed to have the form suggested by Long (1974), according to which the collision-coagulation process is active only when the size of larger particles exceeds 50μm. In the present model we adopt the numerical schemes of Bott (1989) for calculating the condensation process and Bott (1998) for collision-coagulation process because of their numerical stability, conservative property and positive definiteness. The gravitational settling process for liquid water particles is also incorporated into the model by assuming the terminal fall velocity as a function of particle size.

We perform a two-dimensional numerical experiment to generate a low-level water cloud by giving a horizontally homogeneous initial condition

with the stable layer above around 1km and convectively unstable layer in lower atmosphere. The vertical shear of horizontal wind is also given in the initial condition. We initially assume the Junge-type size distribution function for aerosol particle as

$$f_{aero}(z,r) = f_0(z)\left(\frac{r}{r_0}\right)^{-3},$$

where r_0 = 0.1μm and f_0 (z) is given as an exponential decay profile as

$$f_0(z) = f_{sfc}\exp\left(-\frac{z}{H}\right), \qquad (2)$$

where f_{sfc} and H denote the value of f_0 at ground level and the scale height, respectively. We assumed the various values of f_{sfc} ranging from f_{sfc}=10^5 m^{-3} to 10^7 m^{-3} for investigating the aerosol effect on the cloud property, and the scale height H was set to 1km. Values of f_{sfc}=10^5 m^{-3} and 10^7 m^{-3} approximately correspond to aerosol number concentration of n_a=10^8 m^{-3} and 10^{10} m^{-3}, respectively, and also to column aerosol particle numbers of N_a=10^{11} m^{-2} and 10^{13} m^{-2}, respectively, with the 1 km scale height. A warm-bubble is initially located to trigger convection and cloud formation. The computational domain is set as 30km in horizontal and 5km in vertical, and the resolutions are 500m in horizontal and 50m in vertical.

We divide the cloud size distribution ranging from 3μm to 3000μm into three parts, i.e. 3-30μm, 30-300μm and 300-3000μm, and represent each range as cloud, drizzle, and rain water part, respectively. The mass concentrations of cloud, drizzle, and rain can be calculated by integrating the simulated size distribution over these ranges. Also, we explicitly calculate the optical thickness and effective radius from the simulated size distribution function f (x,z,r) for each grid point (x,z) by their definitions as

$$\tau_c(x) = \int_{z=z_B}^{z=z_T}\int_{r=3\mu m}^{r=30\mu m} Q_{ext} f(x,z,r)\pi r^2 dr dz,$$

$$r_e(x,z) = \frac{\int_{r=3\mu m}^{r=30\mu m} f(x,z,r)r^3 dr}{\int_{r=3\mu m}^{r=30\mu m} f(x,z,r)r^2 dr},$$

where Q_{ext} is the extinction coefficient factor and equals to 2 in good approximation for cloud particles, and z_B and z_T denotes the cloud base and cloud top, respectively. Because the remotely sensed value of r_e is largely determined by the size of cloud particles in the upper layer of the total optical thickness (Nakajima and King, 1990), we adopt the calculated value of r_e at the equivalent height with the remote sensing. We determine the equivalent height by the method described in Nakajima and King (1990) except for the expression of the diffusion exponent at 3.7μm developed by Nakajima and Nakajima (1995) for comparing with their results.

We also calculated the column-averaged effective radius in same manner as satellite remote sensing works (Masunaga et al., 2002b; Matsui et al., 2004) as follows:

$$r_e(column) = \frac{2}{3}\frac{1}{\rho_w}\frac{W}{\tau_c},$$

where W denotes the microwave-retrieved liquid water path, which is calculated in the model as follows:

$$W = \rho_w \frac{4}{3}\pi\int_{z=z_B}^{z=z_T}\int_{r=3\mu m}^{r=300\mu m} f(x,z,r)r^3 dr dz,$$

where ρ_w denotes a liquid water density. Because W thus calculated contains the mass of drizzle water, r_e(column) has the signal of drizzle particles.

3. Result and Discussion

Figure 1 shows a scatter plot of effective radius and optical thickness obtained from the simulation. The value of f_{sfc}, assumed in equation (2), is changed from f_{sfc}=10^5 m^{-3} to f_{sfc}= 10^7 m^{-3}., approximately corresponding to n_a=10^8 m^{-3} and 10^{10} m^{-3}, respectively. Simulated results for the condition of n_a smaller than 10^9 m^{-3} (pristine condition) are shown in the upper panel of Figure 1 and the results for n_a greater than 10^9 m^{-3} (polluted condition) are shown in the lower panel of Figure 1. Each point in Figure 1 represents the cloud state at a particular time and a particular spatial grid.

There is a distinctive difference between the simulated scatter plots for pristine and polluted conditions. The scatter plot for pristine condition (Figure 1 upper panel) has a large portion of negative correlation with only a small part of positive correlation, whereas the scatter plot for polluted condition (Figure 1 lower panel) has only a positive correlation branch. Former and latter features closely resemble the observed characteristics over FIRE and ASTEX regions, respectively, obtained from satellite remote sensing by Nakajima and Nakajima (1995).

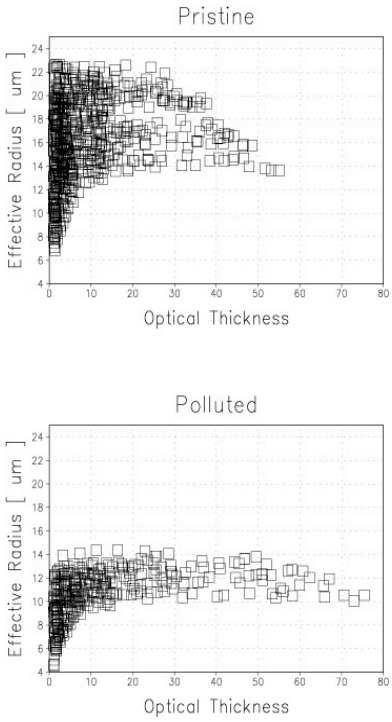

Fig.1: Scatter plots of effective radius and optical thickness obtained from the simulation for pristine (upper panel) and polluted (lower panel) air condition.

The scatter plot for pristine condition shown in the upper panel of Figure 1 is characterized by a large portion of negative correlation with lack of positive correlation part except for a small segment. These characteristics are very similar to those observed over the FIRE region off California by Nakajima and Nakajima (1995). In this case the cloud becomes optically thicker with particle growth indicated by the small part of positive correlation at the early stage before drizzling, followed by active formation of drizzle particles illustrated by the large portion of negative correlation.

In the polluted case shown in the lower panel of Figure 1, on the contrary, only a positive correlation is found, indicating that non-drizzling clouds are dominant in this case. Under the polluted condition, abundant aerosol particles produce numerous cloud particles and the super saturation is limited to lower values due to large consumption of water vapor by condensation of numerous cloud particles. The low value of supersaturation delays the condensational growth as given by equation (1) and thus the cloud particle cannot reach a size enough to activate the collision-coagulation process. This is the reason why we have only the positive correlation branch for polluted condition. This positively correlated feature is also found in the scatter plot obtained from satellite observation over ASTEX region of North Atlantic Ocean by Nakajima and Nakajima (1995).

It is concluded from the above discussion that the correlation pattern between optical thickness and effective radius is significantly affected by aerosol amount and the simulated correlation patterns for pristine and polluted condition have closely similar features to satellite observation over FIRE and ASTEX regions, respectively. This fact suggests that the satellite-observed difference in r_e-τ_c correlation pattern between FIRE and ASTEX regions can be explained by a difference in the aerosol amount over these regions. In fact it is known from satellite observation of aerosols (e.g. Husar et al., 1997; Higurashi and Nakajima, 1999) that the aerosol amount over FIRE and ASTEX region is distinctively different, that is, the FIRE region is comparatively pristine and the ASTEX region is polluted. Such difference in the aerosol burden causes the different growth patterns of cloud particles as depicted by the contrast of r_e-τ_c correlation patterns in our model simulation.

We also investigated the correlation pattern between column-averaged effective radius r_e(column) and the effective radius near the cloud top r_e(top) as shown in Figure 2. It is illustrated in Figure 2 that the r_e(column) generally tends to increase with r_e(top) as expected from the particle growth process.

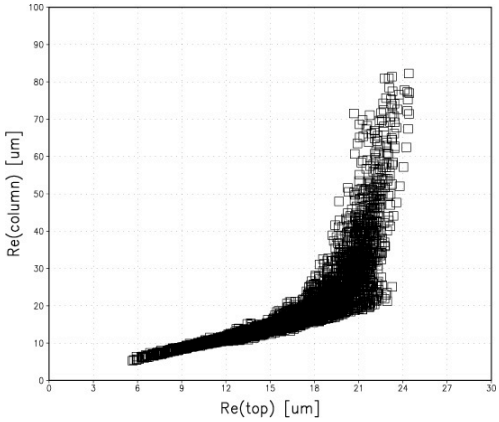

Fig. 2: Scatter plot of r_e(column) and r_e(top) obtained from the simulation.

The remarkable feature found in Figure 2 is a transition of correlation curve, that is, the slow increase in r_e(column) with r_e(top) over the range of small particles of r_e(top) < 15μm and the rapid increase in r_e(column) with r_e(top) over the range of

large particles of r_e(top) > 15μm. The slow increase region for r_e(top) < 15μm is formed by condensational growth process, which is dominant in non-drizzling clouds, and the tendency of rapid increase for r_e(top) > 15μm is formed by collision-coagulation growth process, which is dominant in drizzling clouds. This transitional feature found in the simulated correlation curve between r_e(column) and r_e(top) is similar to the observed characteristics obtained from the satellite remote sensing works by Matsui et al. (2004). They investigated a global statistics of r_e(column) and r_e(top) derived from the TRMM analysis and found the transition of correlation curve around r_e(top)=15μm, similar to our model result shown in Figure 2.

4. Conclusion

In this study we performed the numerical simulation of water cloud optical properties with a spectral bin microphysics cloud model, and investigated the correlation pattern between effective radius and optical thickness. It was revealed that the simulated r_e-τ_c correlation pattern is significantly affected by aerosol amount. The correlation pattern for pristine condition resembles the satellite-observed one over FIRE region off California, in which the negative correlation is dominant, accompanied by a small portion of positive correlation. The simulated correlation for polluted condition, on the contrary, reproduced the similar feature to satellite observation over ASTEX region of North Atlantic Ocean, dominated by positive correlation. It is suggested that the observed difference in the r_e-τ_c correlation pattern can be interpreted as the manifestation of difference in cloud microstructure induced by the different aerosol amount over these regions.

We also simulated the correlation pattern between column-averaged effective radius r_e(column) and the effective radius near the cloud top r_e(top). The transition of correlation curve around the critical value of r_e(top)=15μm is simulated similar to the satellite-observed feature obtained by TRMM global analysis. It is implied that the satellite-observed correlation pattern between r_e(column) and r_e(top) is a global manifestation of particle growth process.

References

Asano, S., M. Shiobara, and A. Uchiyama, 1995: Estimation of cloud physical parameters from airborne solar spectral reflectance measurements for stratocumulus clouds, *J. Atmos. Sci.*, **52**, 3556-3576.

Boers R., and L. D. Rotstayn, 2001: Possible links between cloud optical depth and effective radius in remote sensing observations, *Q. J. R. Meteorol. Soc.*, **127**, 2367-2383.

Bott, A., 1998: A positive definite advection scheme obtained by nonlinear renormalization of the advective fluxes, *Mon. Wea. Rev.*, **117**, 1006-1015.

Bott, A., 1998: A flux method for the numerical solution of the stochastic collection equation, *J. Atmos. Sci.*, **55**, 2284-2293.

Brenguier, J-L., H. Pawlowska, L. Schuller, R. Preusker, J. Fischer, and Y. Fouquart, 2000: Radiative properties of boundary layer clouds: Droplet effective radius versus number concentration, *J. Atmos. Sci.*, **57**, 803-821.

Han, Q., W. B. Rossow, and A. A. Lacis, 1994: Near-global survey of effective droplet radii in liquid water clouds using ISCCP data, *J. Climate*, **7**, 465-497.

Han, Q., W. B. Rossow, J. Chou, and R. M. Welch, 1998: Global survey of the relationships of cloud albedo and liquid water path with droplet size using ISCCP, *J. Climate*, **11**, 1516-1528.

Higurashi A., and T. Nakajima, 1999: Development of a two-channel aerosol retrieval algorithm on a global scale using NOAA AVHRR, *J. Atmos. Sci.*, **56**, 924-941.

Husar, R. B., J. M. Prospero, and L. L. Stowe, 1997: Characterization of tropospheric aerosols over the oceans with the NOAA advanced very high resolution radiometer optical thickness operational product, *J. Geophys. Res.*, **102(D14)**, 16889-16909.

Kawamoto, K., T. Nakajima, and T. Y. Nakajima, 2001: A global determination of cloud microphysics with AVHRR remote sensing, *J. Climate*, **14**, 2054-2068.

Khain, A., A. Pokrovsky, A. Pinsky, A. Seifeld, and V. Phillips, 2004: Simulation of effects of atmospheric aerosols on deep turbulent convective clouds using a spectral microphysics mixes-phase cumulus cloud model. Part I: Model description and possible applications. *J. Atmos. Sci.*, **61**, 2963-2982.

Khain, A., and I. Sednev, 1996: Simulation of precipitation formation in the Eastern Mediterranean coastal zone using a spectral microphysics cloud ensemble model. *Atmos. Res.*, **43**, 77-110.

Long, A. B., 1974: Solutions to the droplet collection equation for polynomial kernels, *J. Atmos. Sci.*, **31**, 1040-1052.

Masunaga, H., T. Y. Nakajima, T. Nakajima, M. Kachi, R. Oki, and S. Kuroda, 2002a: Physical properties of maritime low clouds as retrieved by combined use of Tropical Rainfall Measuring Mission Microwave

Imager and Visible/Infrared Scanner: Algorithm. *J. Geophys. Res.*, **107**, 10.1029/2001JD000743.

Masunaga, H., T. Y. Nakajima, T. Nakajima, M. Kachi, and K. Suzuki, 2002b: Physical properties of maritime low clouds as retrieved by combined use of Tropical Rainfall Measuring Mission Microwave Imager and Visible/Infrared Scanner. II. Climatology of warm clouds and rain. *J. Geophys. Res*., **107**, 4367, doi:10.1029/2001JD001269.

Matsui, T., H. Masunaga, R. A. Pielke Sr., and W.-K. Tao, 2004: Impact of aerosols and atmospheric thermodynamics on cloud properties within the climate system, *Geophys. Res. Lett*., **31**, L06109, doi:10.1029/2003GL019287.

Nakajima, T., and M. D. King, 1990: Determination of the optical thickness and effective particle radius of clouds from reflected solar radiation measurements. Part I: Theory. *J. Atmos. Sci*., **47**, 1878-1893.

Nakajima, T., M. D. King, and J. D. Spinhirne, 1991: Determination of the optical thickness and effective particle radius of clouds from reflected solar radiation measurements. Part II: Marine stratocumulus observations. *J. Atmos. Sci*., **48**, 728-750.

Nakajima, T. Y., and T. Nakajima, 1995: Wide-area determination of cloud microphysical properties from NOAA AVHRR measurements for FIRE and ASTEX regions. *J. Atmos. Sci*., **52**, 4043-4059.

Peng, Y., U. Lohmann, R. Leaitch, C. Banic, and M. Couture, 2002: The cloud albedo-cloud droplet effective radius relationship for clean and polluted clouds from RACE and FIRE.ACE. *J. Geophys. Res*., **107(D11)**, 4106, 10.1029/2000JD000281.

Rogers, R. R., and M. K. Yau, 1989: *A Short Course in Cloud Physics*. 3rd edition, Pergamon Press, 293pp.

Szczodrak, M., P. H. Austin, and P. B. Krummel, 2001: Variability of optical depth and effective radius in marine stratocumulus clouds, *J. Atmos. Sci*., **58**, 2912-2926.